Sn-inserted Al-induced layer exchange for large-grained GeSn thin films on insulator

Kaoru Toko*, Naoki Oya, Mitsuki Nakata, and Takashi Suemasu

Institute of Applied Physics, University of Tsukuba, 1-1-1 Tennodai, Tsukuba, Ibaraki 305-8573, Japan

E-mail: toko@bk.tsukuba.ac.jp

Large-grained polycrystalline GeSn layers on glass are achieved through the layer exchange between a-Ge and Sn-doped Al layers. The thicker Sn layers, inserted below Al layers, provided the faster growth velocity, resulting in the smaller grain size of the GeSn layer. Controlling the Sn thickness (10 nm) and the growth temperature (300 °C) allowed for approximately 80% (111)-oriented GeSn layer with grains having an average size of 40 μm. The lower growth temperature led to the higher Sn content in GeSn: 300 °C resulted in a Sn content of 2%. These findings are meaningful to researches related to GeSn on insulators for fabricating advanced electrical and optical devices on inexpensive substrates as well as on Si platforms.

Keywords: Metal-induced crystallization; Al-induced layer exchange; Crystal orientation; Solid phase crystallization; Polycrystalline films; Semiconducting germanium

1. Introduction

GeSn offers exciting possibilities as a next-generation material for advanced electronic and photonic devices based on group-IV semiconductors [1,2]. Although the solubility limit of Sn in Ge is as low as 1%, non-equilibrium low-temperature process using molecular-beam epitaxy (MBE) [3-6], chemical-vapor deposition (CVD) [7,8], or ion implantation [9] have allowed for Sn contents more than the solubility limit. These studies have demonstrated the advantage of GeSn: the carrier mobility of GeSn exceeded that of Ge [10,11]; the infrared detection capability, covering all the relevant telecommunications wavelengths, is extended by Sn contents over 2% [12-14]; high substitutional Sn content (> 6%) in GeSn provides the direct transition in the near infrared region, allowing for lasing [15,16].

The study of GeSn on insulators (GSOIs) has been accelerated for fabricating monolithically integrated GeSn-based devices on three-dimensional Si large-scale integrated circuits and on multi-functional displays with glass or plastic substrates [17-26]. The incorporation of 2% Sn into Ge passivated the vacancy defects or reduced the grain boundary scattering, resulting in the higher carrier mobilities than Ge [18,19]. The tin-induced crystallization (TIC) of amorphous Ge (a-Ge) has recently garnered attention [23-26]. We controlled the Sn content in the resulting polycrystalline (poly-) GeSn by tuning the TIC temperature and achieved high-Sn (25%) content poly-GeSn on glass at 70 °C [26]. The grain sizes of the poly-GeSn layers formed by TIC, however, were small (< 1 μm), which would deteriorate the electrical properties of the GeSn layer.

For fabricating a large-grained (> 100 μm) poly-Ge on insulators, layer exchange growth between metal and a-Ge layers has been widely investigated using Al [27-31] or Au

[32-33]. Besides, the layer exchange technique enables us to form (111)-oriented Ge [31-33], which is preferable for Ge devices [34,35]. In the preset paper, we studied a way using Sn-doped Al-induced crystallization (AIC) to form a large-grained, (111)-oriented poly-GeSn thin film on an insulator. The Sn-doping facilitated the growth and resulted in a 2% Sn-content GeSn layer with 40 μm grains.

2. Experimental details

Figure 1 shows the process of sample preparation. The Sn (thickness: 0-20 nm) and Al (thickness: 50 nm) layers were prepared in sequence on SiO_2 glass substrates. After the depositions, the Al layers were exposed to air for 10 min to form native AlO_x membranes as diffusion limiting layers, which significantly influence the growth properties of AIC. From our previous study, the thickness of the AlO_x membrane is estimated to be approximately 2 nm [29]. After that, 60-nm-thick undoped a-Ge layers were prepared. All depositions were carried out at room temperature using a radio-frequency magnetron sputtering method. The samples were then annealed at 300-350 °C for 100 h in N_2 ambient. Here we expected the following reactions: the Sn and Al layers were mixed each other during annealing because the Sn-Al eutectic point is 231 °C, and then the a-Ge layer is crystallized in GeSn via the layer exchange, as schematically shown in Fig. 1.

After the completion of the layer exchange, the Ge islands and Al layer, remaining in the top layer, are sequentially removed using 50% H_2O_2 solution for 30 min and 1.5% HF solution for 1 min [31]. The resulting layers were characterized by using Nomarski optical microscopy, a θ-2θ X-ray diffraction (XRD) measurement (spot size: 10 mm), and electron backscatter diffraction (EBSD) analysis.

3. Results and discussion

Figure 2 shows Nomarski optical micrographs of the back surfaces of the 300 °C annealed samples with and without a 10-nm-thick Sn layer. As representatively shown in Fig. 2, at 300 °C, the layer exchange of the samples with the thin Sn layers (0-5 nm) did not finish within 100 h, while that of the samples with the thick Sn layers (10-20 nm) finished. These results mean that the growth velocity increased with increasing the initial Sn thickness. This behavior, i.e., the growth velocity enhancement of a-Ge using Sn as a catalyst, is consistent with the previous reports [25,26]. This is because the temperature of the reaction between Sn and a-Ge is quite low. On the other hand, at 350 °C, the samples with the thick Sn layers (> 10 nm) led to the crystallization of a-Ge without layer exchange, resulting in fine grains (< 1 μm) according to the EBSD measurement. This is likely owing to the diffusion of Sn into the a-Ge layer, which crystallized the a-Ge layer before layer exchange started. Note that the thickness of the resulting Ge(Sn) layer was the same as the total thickness of the initial Al and Sn layers. The surface roughness of the Ge(Sn) was measured using atomic force microscopy. The root mean square value was found to be 4.3 nm, which was almost the same as that of the Al layer stacked on the Sn layer before annealing. These results suggest that the mixed Al-Sn layer acted as a catalyst for layer exchange growth of a-Ge [30].

Figure 3 shows the EBSD images of the samples grown via layer exchange, indicating that the crystal orientation of the resulting Ge(Sn) layers is significantly affected by the Sn insertion as well as the growth temperature. Figures 3(a) and 3(c) show that the samples without Sn layers are highly (111)-oriented, consistent with our prior studies using

91 50-nm-thick Al layers [29,30]. When the Sn layers are inserted, the resulting Ge(Sn) layers
92 have (100)-oriented regions. This phenomenon is pronounced for the samples with thicker
93 Sn layers and higher growth temperatures, as shown in Figs. 3(b), 3(e), and 3(f). Thus, the
94 AIC-Ge(Sn) layers are (111)- or (100)-oriented. This behavior is the same as AIC-Si, where
95 the interfacial energy of Si nuclei in Al becomes minimum in (111) or (100) planes
96 depending on the growth conditions [36]. By tuning the Sn thickness and growth
97 temperatures, (111)-oriented Ge layers can be obtained, as shown in Figs. 3(d) and 3(g).
98 The crystal orientation fraction and the average grain size of the resulting Ge(Sn)
99 layers were estimated from the EBSD images shown in Fig. 3. Figures 4(a)-4(c)
100 respectively indicate that the thicker Sn layer provides the lower (111) orientation fraction,
101 the higher (100) orientation, and the smaller grain size. This is a typical behavior when the
102 growth velocity in AIC is promoted [37,38]: the insertion of the Sn layer likely facilitated
103 the nucleation other than (111) orientation, and reduced the size of the resulting grains.
104 Thus, by lowering the growth temperature, i.e., lowering the growth velocity, the (111)
105 orientation and the grain size are improved. For all the samples grown via the layer
106 exchange, the grain sizes are no less than 20 μm, which is large enough for device
107 fabrications.
108 The Sn content in the resulting layers was evaluated by using a θ-2θ XRD
109 measurement. Figure 5 (a) shows the XRD patterns of the samples annealed at 325 °C. The
110 peaks at around 27°, originated from the Ge(111) plane, are observed for all the samples. In
111 the measured 2θ range (20-60°), other peaks were not observed because the poly-GeSn
112 layers were thin and preferentially (111)-oriented. With increasing the thickness of the
113 inserted Sn layer, the peak intensity is further weakened. This behavior is attributed to the
114 lower (111) orientation fraction, as shown in Fig. 4(a). The detailed analysis clarified that

115 the peak positions of the samples with a Sn layer slightly shifted to smaller angles,
116 suggesting the formation of GeSn containing substitutional Sn atoms [26]. The Sn contents
117 were calculated from the peak positions assuming the validity of Vegard's law. The results
118 are shown in Fig. 5(b). When the Sn layer is thin, the Sn content in GeSn increases as the
119 Sn thickness increases. On the other hand, when the Sn layer is thick, the Sn content in
120 GeSn is constant regardless of the Sn thickness. The saturated Sn content is determined by
121 the annealing temperature: the lower temperature provides the higher Sn content. The
122 maximum Sn content of 2% was obtained at 300 °C. We evaluated the electrical properties
123 of the poly-GeSn, formed at 300 °C with a 10-nm-thick Sn layer, using Hall measurement.
124 The carrier mobility was 20 cm^2/Vs and the hole concentration was 3.5×10^{20} cm^{-3}. These
125 values are almost the same as those of the Al-doped Ge layer formed by conventional AIC.
126 Figure 5 (c) shows that the Sn content clearly increases with decreasing the annealing
127 temperatures and that the result of AIC-GeSn is consistent with that of TIC-GeSn [26] on
128 the perspective of the relationship between the Sn content and growth temperature. These
129 results suggest that the maximum Sn content in GeSn is limited by the growth temperature
130 when the GeSn is formed as a result of the reaction between Sn and a-Ge. This is because
131 that the saturated Sn concentration is likely determined by both the solubility limit of Sn in
132 Ge (approximately 1%) and the non-equilibrium fluctuation, depending on the process
133 temperature. Lowering the growth temperature in AIC using growth promotion techniques,
134 reported in Ref. 30, will yield a large-grained GeSn layer with a higher Sn content.
135

136 4. Conclusions

137 The Sn-doped AIC of a-Ge, initially inserting Sn layers below Al, was

investigated to obtain a large-grained GeSn layer on insulators. Thickening the Sn layer facilitated the growth velocity of AIC, deteriorating the grain size and (111) orientation fraction of the resulting GeSn layer. By tuning the thickness of the Sn layer (10 nm) and the growth temperature (300 °C), a large-grained (~40 μm), (111)-oriented (~80%) GeSn layer on glass was achieved. Those growth properties are the advantages over the previous poly-GeSn layers formed by the solid-phase crystallization of a-GeSn. The Sn content in the GeSn layer was 2%, which was determined by the growth temperature. These findings are meaningful to the research on GSOIs for fabricating high-performance electrical and optical devices on inexpensive substrates.

Acknowledgments

This work was financially supported by the JGC-S Scholarship Foundation and the Japan Prize Foundation. Some experiments were conducted at the International Center for Young Scientists in NIMS.

152 ## References

153 [1] K. Alberi, J. Blacksberg, L. Bell, S. Nikzad, K. Yu, O. Dubon, W. Walukiewicz, Band anticrossing in
154 highly mismatched Sn_xGe_{1-x} semiconducting alloys, Phys. Rev. B **77** (2008) 073202.
155 [2] W.-J. Yin, X.-G. Gong, S.-H. Wei, Origin of the unusually large band-gap bowing and the breakdown of
156 the band-edge distribution rule in the Sn_xGe_{1-x} alloys, Phys. Rev. B **78** (2008) 161203.
157 [3] Y. Shimura, N. Tsutsui, O. Nakatsuka, A. Sakai, S. Zaima, Low temperature growth of $Ge_{1-x}Sn_x$ buffer
158 layers for tensile–strained Ge layers, Thin Solid Films **518** (2010) S2.
159 [4] M. Oehme, K. Kostecki, M. Schmid, M. Kaschel, M. Gollhofer, K. Ye, D. Widmann, R. Koerner, S.
160 Bechler, E. Kasper, J. Schulze, Franz-Keldysh effect in GeSn pin photodetectors, Appl. Phys. Lett. **104**
161 (2014) 161115.
162 [5] H. Lin, R. Chen, Y. Huo, T. I. Kamins, J. S. Harris, Raman study of strained $Ge_{1-x}Sn_x$ alloys, Appl. Phys.
163 Lett. **98** (2011) 261917.
164 [6] A. A. Tonkikh, N. D. Zakharov, A. A. Suvorova, C. Eisenschmidt, J. Schilling, P. Werner, Cubic Phase
165 Sn-Rich GeSn Nanocrystals in a Ge Matrix, Cryst. Growth Des. **14** (2014) 1617.
166 [7] V. R. D'Costa, J. Tolle, R. Roucka, C. D. Poweleit, J. Kouvetakis, J. Menéndez, Raman scattering in
167 $Ge_{1-y}Sn_y$ alloys, Solid State Commun. **144** (2007) 240.
168 [8] B. Vincent, F. Gencarelli, H. Bender, C. Merckling, B. Douhard, D. H. Petersen, O. Hansen, H. H.
169 Henrichsen, J. Meersschaut, W. Vervorst, M. Heyns, R. Loo, M. Caymax, Undoped and in-situ B doped
170 GeSn epitaxial growth on Ge by atmospheric pressure-chemical vapor deposition, Appl. Phys. Lett. **99**
171 (2011) 152103.
172 [9] K. Gao, S. Prucnal, R. Huebner, C. Baehtz, I. Skorupa, Y. Wang, W. Skorupa, M. Helm, S. Zhou, $Ge_{1-x}Sn_x$
173 alloys synthesized by ion implantation and pulsed laser melting, Appl. Phys. Lett. **105** (2014) 042107.
174 [10] S. Gupta, Y. Huang, Y. Kim, E, Sanchez, K. C. Saraswat, Hole mobility enhancement in compressively
175 strained $Ge_{0.93}Sn_{0.07}$ pMOSFETs, IEEE Electron Device Lett. **34** (2013) 831.
176 [11] R. R. Lieten, T. Maeda, W. Jevasuwan, H. Hattori, N. Uchida, S. Miura, M. Tanaka, J.-P. Locquet,
177 Tensile-Strained GeSn Metal–Oxide–Semiconductor Field-Effect Transistor Devices on Si(111) Using Solid
178 Phase Epitaxy, Appl. Phys. Express **6** (2013) 101301.
179 [12] J. Mathews, R. Roucka, J. Xie, S. Q. Yu, J. Menendez, J. Kouvetakis, Extended performance

180 GeSn/Si(100) *p-i-n* photodetectors for full spectral range telecommunication applications, Appl. Phys. Lett.
181 **95** (2009) 133506.
182 [13] Y. Nakamura, N. Fujinoki, M. Ichikawa, Photoluminescence from Si-capped GeSn nanodots on Si
183 substrates formed using an ultrathin SiO_2 film technique, J. Appl. Phys. **106** (2009) 014309.
184 [14] H. H. Tseng, H. Li, V. Mashanov, Y. J. Yang, H. H. Cheng, G. E. Chang, R. A. Soref, G. Sun,
185 GeSn-based p-i-n photodiodes with strained active layer on a Si wafer, Appl. Phys. Lett. **103** (2013) 231907.
186 [15] P. Moontragoon, R. A. Soref, Z. Ikonic, The direct and indirect bandgaps of unstrained $Si_xGe_{1-x-y}Sn_y$ and
187 their photonic device applications, J. Appl. Phys. **112** (2012) 073106.
188 [16] S. Wirths, R. Geiger, N.V. Den Driesch, G. Mussler, T. Stoica, S. Mantl, Z. Ikonic, M. Luysberg, S.
189 Chiussi, J.M. Hartmann, H. Sigg, J. Faist, D. Buca, D. Grützmacher, Lasing in direct-bandgap GeSn alloy
190 grown on Si, Nat. Photonics **9** (2015) 88.
191 [17] O. Nakatsuka, K. Mochizuki, Y. Shimura, T. Yamaha, S. Zaima, Low temperature formation of
192 $Si_{1-x-y}Ge_xSn_y$-on-insulator structures by using solid-phase mixing of $Ge_{1-z}Sn_z$/Si-on-insulator substrates,
193 Thin Solid Films **520** (2012) 3288.
194 [18] O. Nakatsuka, N. Tsutsui, Y. Shimura, S. Takeuchi, A. Sakai, S. Zaima, Mobility behavior of $Ge_{1-x}Sn_x$
195 layers grown on silicon-on-insulator substrates, Jpn. J. Appl. Phys. **49** (2010) 04DA10.
196 [19] W. Takeuchi, N. Taoka, M. Kurosawa, M. Sakashita, O. Nakatsuka, S. Zaima, High hole mobility
197 tin-doped polycrystalline germanium layers formed on insulating substrates by low-temperature solid-phase
198 crystallization, Appl. Phys. Lett. **107** (2015) 022103.
199 [20] M. Kurosawa, Y. Tojo, R. Matsumura, T. Sadoh, M. Miyao, Single-crystalline laterally graded GeSn on
200 insulator structures by segregation controlled rapid-melting growth, Appl. Phys. Lett. **101** (2012) 091905.
201 [21] M. Kurosawa, N. Taoka, H. Ikenoue, O. Nakatsuka, S. Zaima, Large grain growth of Ge-rich $Ge_{1-x}Sn_x$
202 ($x \approx 0.02$) on insulating surfaces using pulsed laser annealing in flowing water, Appl. Phys. Lett. **104** (2014)
203 061901.
204 [22] H. Li, X. Wang, J. Liu, Pseudo single crystal, direct-band-gap $Ge_{0.89}Sn_{0.11}$ on amorphous dielectric layers
205 towards monolithic 3D photonic integration, Appl. Phys. Lett. **105** (2014) 201107.
206 [23] H. Li, J. Brouillet, A. Salas, X. Wang, J. Liu, Low temperature growth of high crystallinity GeSn on
207 amorphous layers for advanced optoelectronics, Opt. Mater. Express **3** (2013) 1385.

208 [24] M. Kurosawa, N. Taoka, M. Sakashita, O. Nakatsuka, M. Miyao, S. Zaima, Liquid-Sn-driven lateral
209 growth of poly-GeSn on insulator assisted by surface oxide layer, Appl. Phys. Lett. **103** (2013) 101904.
210 [25] H. Chikita, R. Matsumura, Y. Kai, T. Sadoh, M. Miyao, Ultra-high-speed lateral solid phase
211 crystallization of GeSn on insulator combined with Sn-melting-induced seeding, Appl. Phys. Lett. **105**
212 (2014) 202112.
213 [26] K. Toko, N. Oya, N. Saitoh, N. Yoshizawa, T. Suemasu, 70 °C synthesis of high-Sn content (25%) GeSn
214 on insulator by Sn-induced crystallization of amorphous Ge, Appl. Phys. Lett. **106** (2015) 082109.
215 [27] Z.M. Wang, J.Y. Wang, L.P.H. Jeurgens, F. Phillipp, E.J. Mittemeijer, Origins of stress development
216 during metal-induced crystallization and layer exchange: Annealing amorphous Ge/crystalline Al bilayers,
217 Acta Mater. **56** (2008) 5047.
218 [28] S. Hu, A.F. Marshall, P.C. McIntyre, Interface-controlled layer exchange in metal-induced crystallization
219 of germanium thin films, Appl. Phys. Lett. **97** (2010) 082104.
220 [29] K. Toko, M. Kurosawa, N. Saitoh, N. Yoshizawa, N. Usami, M. Miyao, T. Suemasu, Highly
221 (111)-oriented Ge thin films on insulators formed by Al-induced crystallization, Appl. Phys. Lett. **101** (2012)
222 072106.
223 [30] K. Toko, R. Numata, N. Oya, N. Fukata, N. Usami, T. Suemasu, Low-temperature (180 °C) formation of
224 large-grained Ge (111) thin film on insulator using accelerated metal-induced crystallization, Appl. Phys.
225 Lett. **104** (2014) 022106.
226 [31] K. Toko, K. Nakazawa, N. Saitoh, N. Yoshizawa, T. Suemasu, Improved Surface Quality of the
227 Metal-Induced Crystallized Ge Seed Layer and Its Influence on Subsequent Epitaxy, Cryst. Growth Des. **15**
228 (2015) 1535.
229 [32] J.-H. Park, K. Kasahara, K. Hamaya, M. Miyao, T. Sadoh, High carrier mobility in orientation-controlled
230 large-grain (≥50 μm) Ge directly formed on flexible plastic by nucleation-controlled
231 gold-induced-crystallization, Appl. Phys. Lett. **104** (2014) 252110.
232 [33] H. Higashi, K. Kasahara, K. Kudo, H. Okamoto, K. Moto, J.-H. Park, S. Yamada, T. Kanashima, M.
233 Miyao, I. Tsunoda, K. Hamaya, A pseudo-single-crystalline germanium film for flexible electronics, Appl.
234 Phys. Lett. **106** (2015) 041902.
235 [34] T. Sasada, Y. Nakakita, M. Takenaka, S. Takagi, Surface orientation dependence of interface properties of

236 GeO_2/Ge metal-oxide-semiconductor structures fabricated by thermal oxidation, J. Appl. Phys. **106** (2009)
237 073716.
238 [35] T. Nishimura, C. H. Lee, T. Tabata, S. K. Wang, K. Nagashio, K. Kita, A. Toriumi,
239 High-Electron-Mobility Ge n-Channel Metal–Oxide–Semiconductor Field-Effect Transistors with
240 High-Pressure Oxidized Y_2O_3, Appl. Phys. Express **4** (2011) 064201.
241 [36] A. Sarikov, J. Schneider, J. Berghold, M. Muske, I. Sieber, S. Gall, et al., A kinetic simulation study of
242 the mechanisms of aluminum induced layer exchange process, J. Appl. Phys. **107** (2010) 114318.
243 [37] K. Toko, R. Numata, N. Saitoh, N. Yoshizawa, N. Usami, T. Suemasu, Selective formation of
244 large-grained, (100)- or (111)-oriented Si on glass by Al-induced layer exchange, J. Appl. Phys. **115** (2014)
245 094301.
246 [38] M. Kurosawa, T. Sadoh, M. Miyao, Comprehensive study of Al-induced layer-exchange growth for
247 orientation-controlled Si crystals on SiO_2 substrates, J. Appl. Phys. **116** (2014) 173510.
248

Figure Captions

Fig. 1. Schematic of the sample preparation.

Fig. 2. Nomarski optical micrographs of the back surfaces of the 300 °C annealed samples (a) without and (b) with a 10-nm-thick Sn layer.

Fig. 3. EBSD images of the Ge(Sn) layers in the normal direction, summarized as a matrix of the initial Sn thickness (0, 5, 10, and 20 nm) and the annealing temperature (300, 325, and 350 °C). The coloration indicates crystal orientation, as shown in the legend.

Fig. 4. Initial Sn thickness dependence of (a) (111) orientation fraction, (b) (100) orientation fraction, and (c) average grain size in the AIC-GeSn layers annealed at 300 °C (circles), 325 °C (squares), and 350 °C (triangles) for 100 h.

Fig. 5. (a) θ-2θ XRD patterns of the AIC-GeSn layers with initial Sn thickness of 0-20 nm after annealed at 325 °C for 100 h. (b) Initial Sn thickness dependence of Sn concentration in AIC-GeSn after annealed at 300 °C (circles), 325 °C (squares), and 350 °C (triangles) for 100 h, derived from the XRD peak position of Ge(111) using Vegard's law. (c) Annealing temperature dependence of Sn concentration in AIC-GeSn (open circles) and TIC-GeSn (open circles) from Ref. 26.

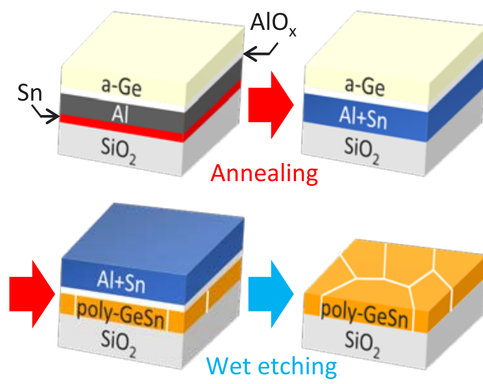

Figure 1

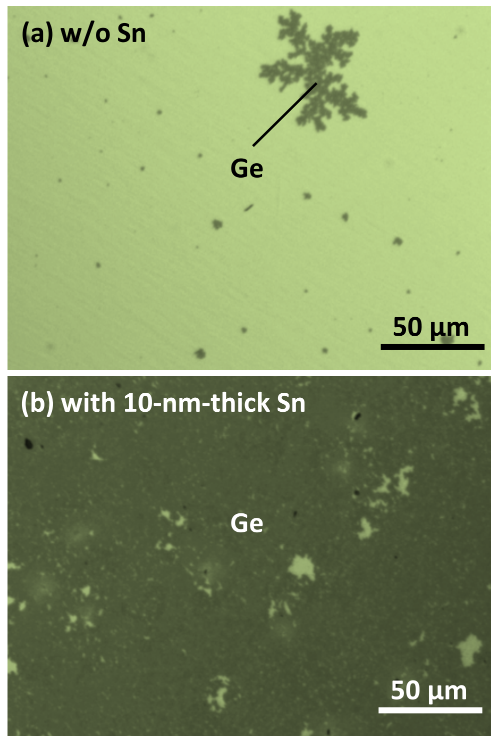

Figure 2

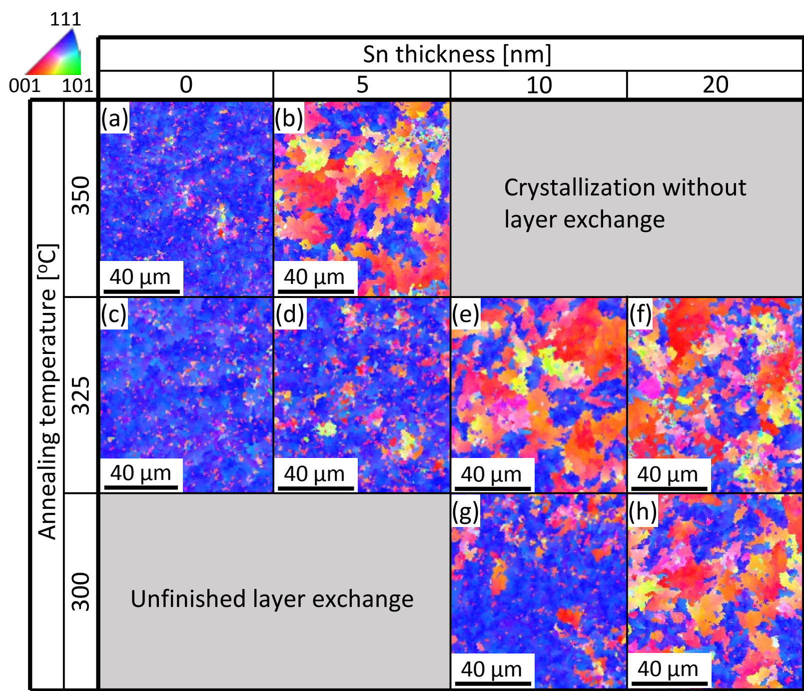

Figure 3

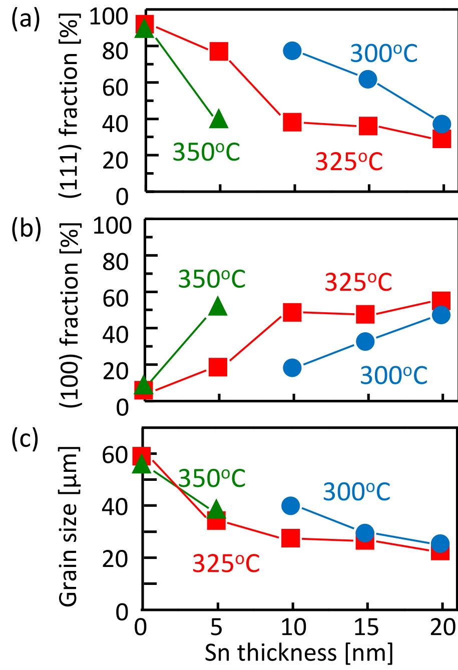

Figure 4

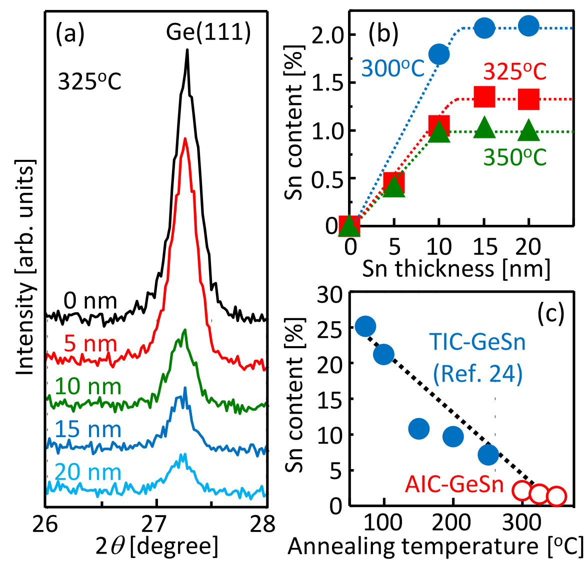

Figure 5